Non-intrusive flowrate measurement and monitoring system of plant-protection unmanned aircraft systems based on pump voice analysis

Yang Xu[1,2], Xinyu Xue[1,2*], Zhu Sun[1,2], Wei Gu[1,2]

(1. *Nanjing Institute for Agricultural Mechanization, Ministry of Agriculture and Rural Affairs, Nanjing 210014, China*;
2. *Sino-USA Pesticide Application Technology Cooperative Laboratory, Nanjing 210014, China*)

Abstract: Application of Unmanned Aircraft Systems (UAS) for plant protection is becoming a common tool in agricultural field management.   To avoid shortcomings of intrusive flowrate sensors including poor measurement accuracy and poor anti-vibration ability, a non-intrusive flowrate measurement and monitoring system of plant-protection UAS was developed based on pump voice signal analysis.   It is mainly composed of STM32 processor, microphone and signal-conditioning circuit. By collecting and analyzing the voice signal of the pump in the UAS, the monitoring system will output the real-time values of spraying flowrate and amount.   An extraction model was developed to determine operation status and primary frequency of the pump based on voice signal analysis.   Real-time spray flowrate can be determined from the real-time extracted primary frequency and the fitted correlation formulas of spraying flowrate under outlet area and pump primary frequency.   The flowrate correlation equation of one certain pump from 4-rotor UAS 3WQFTX-1011S was obtained, the max deviation rate of fitted spray flowrate was only 2.8%.   In primary frequency extraction test, the error rate of primary frequency extraction was less than 1%.   In the 4-rotor UAS flight tests: the max deviation of operating starting/end point was only 0.7 s and the max deviation of extracted total operating time was only 0.8 s; the deviation of extracted spray flowrate was less than 2%, and the max deviation rate of total spray amount was 3.2%.   This research could be used as a guidance for plant-protection UAS non-intrusive flowrate measurement and monitoring.
Keywords: plant protection UAS, voice signal analysis, non-intrusive, flowrate measurement, monitoring system
DOI: 10.25165/j.ijabe.20211403.5508

1   Introduction

With rapid development of aviation plant protection science technology in Asia, Unmanned Aerial Systems (UAS) is playing a more and more import role in plant protection[1,2].   Xue et al.[3] developed an UAS based automatic aerial spraying system, to perform plant-protection operations.   Qin et al.[4] studied the influence of spraying parameters, such as operation height and operation velocity, of the UAS on droplet deposition on the rice canopy and protection efficacy.   Yallappa and Veerangouda[5] developed and evaluated the UAS mounted sprayer for pesticide applications to crops.   Iwasaki and Torita[6] evaluated the spatial pattern of windbreak effects on maize growth using UAS. Different from ground machinery, plant protection UAS does not require dedicated spot for take-off and landing, it embraces short turning radius and causes no damage to crops during operation. More importantly, it can be applied in complex terrain including hills, mountains, slopes and paddy fields.   In the last decade, Research on plant protection UAS is concentrated on UAS operation parameters optimization[7,8], variable-rate spray

technology[9,10], droplets deposition distribution tests[11,12], downwash airflow simulation[13-15] and high resolution-based remote sensing applications[16,17].   To the year of 2018, China owns over 30 000 plant protection UAS.

Currently, intrusive sensors like turbine flowmeter are widely used for UAS spraying flowrate monitoring, provided with poor measurement accuracy, poor anti-vibration ability, poor accessibility to different UAS pipelines and easily blocked due to sedimentations.   Moreover, pesticides corrosiveness reduces the measurement accuracy and service life of those intrusive sensors. As inherent signal emitted by machine, machine voice carries not only the structural information but also the operating status. Through voice signal processing including feature extraction and pattern recognition, online operating status monitoring and faults forecasting of machine can be realized[18-21].   Mannan et al.[22] studied on texture analysis of machined surfaces and signal processing of sound generated by machining process and investigated the correlation between tool wear and quantities characterizing machined surfaces and sound pattern.   Basavaraj et al.[23] approached detection and localization of faults in motorcycles, by exploiting the variations in the spectral behavior.

In this study, a non-intrusive flowrate measurement monitoring system of plant protection UAS was developed based on pump voice signal analysis.   Employing the double-threshold method and the Pauta Criterion, a pump operation status and primary frequency extraction model was proposed.   Real-time spray flowrate and amount was calculated and displayed in the monitoring system, based on the extracted pump status data and fitted flowrate formulas of pump under different outlet area (i.e., nozzles outlet areas) and pump primary frequency (i.e., the rotation

speed of pump motor).

2 Operational principle

The spray system of plant protection Unmanned Aircraft Systems (UAS) is composed of power supply module and spraying implement devices which includes water tank, pump, pipelines and nozzles. At present, most of the plant protection UAS are equipped with low-pressure hydraulic system and single-chamber diaphragm pumps in China[24-26]. The working principle of the single-chamber diaphragm pump is shown in Figure 1.
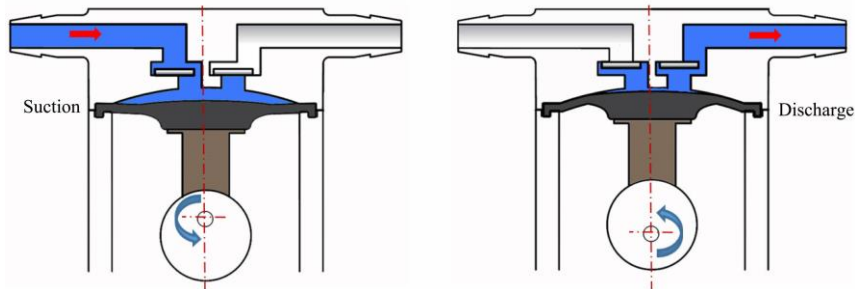

Figure 1　Operational principle of the single-chamber diaphragm pump

When the pressure is zero in the pump ($p=0$), the discharged liquid volume in each diaphragm reciprocation is fixed, i.e., the flowrate of the pump is constant, which is defined as

$$S_{p=0}(f)=f \times V_{p=0} \tag{1}$$

where, $S_{p=0}$ is the pump flowrate when $p=0$, L/min; f is the pump primary frequency (i.e., the rotation speed of pump motor), Hz; $V_{p=0}$ is the volume change for each suction-discharge of the pump when $p=0$. In actual spray operations, different types and numbers of nozzles will be installed in the spraying systems for different requirements. In the hydraulic spraying system, because the pump outlet area A_1 is much larger than the outlet area of the nozzles A_2 (i.e., $A_1 \gg A_2$), pressure will be generated in the pipeline and pump $p=\dfrac{\rho S^2}{g A_2^2}>0$ (0.1-0.4 MPa). Redefine the pressure as

$$p_{re}=\lambda p_{th}(f, A) \tag{2}$$

where, f is the pump primary frequency, Hz; A is the outlet area of the nozzles, mm^2; p_{re} is the actual pressure, MPa; λ is the pressure coefficient; p_{th} is the theoretical pressure, MPa.

The flowrate of the diaphragm pump under pressure is defined as follows

$$S_{re}=A\sqrt{\dfrac{p_{re}g}{\rho}}=\alpha S_{th}(f, A) \tag{3}$$

where, S_{re} is the actual flowrate, L/min; S_{th} is the theoretical flowrate, L/min; α is the flowrate coefficient; g is the gravitational acceleration; ρ is the liquid density inside pump, g/cm^3. It is seen from Equation (3) that pump flowrate is related to pump primary frequency and nozzles outlet area in low-pressure hydraulic system. The actual flowrate formula can be obtained by performing experiments, one specific flowrate formula will be extracted in the section 5.1.

3 System design and data processing

3.1 Pump voice signal collection system design

A STM32-based flowrate monitoring system was designed to acquire the pump voice signal, as shown in Figure 2. The microphone adopted in the design is Adeline-AD20.

Flowrate monitoring system principle diagram is shown in Figure 3. The monitoring system is composed of microphone, signal conditioning circuit, A/D conversion module, power module and 4G module. The sampling frequency is 44.1 kHz. RTK positioning data can be derived combined with flowrate information by connecting RTK module to the STM32 data processor. The microphone is used to convert the pump voice signal to electrical signal. The electrical signal is then converted to digital signal through A/D module after signal conditioning process. The digital signal is processed in STM32 processor and uploaded by 4G module.

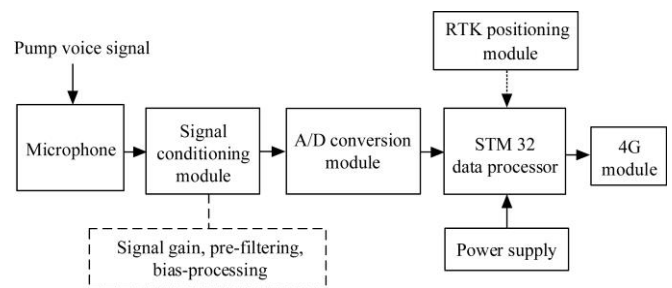Figure 2　STM32-based monitoring system of pump voice signal

Figure 3　Principle diagram of STM32-based monitoring system

3.2 Data processing of pump voice signal

The pump operation status and primary frequency extraction model was designed (Figure 4). The operation time interval can be considered as pre-processing of pump voice signal. Which is determined by setting the energy threshold of pump voice signal at High-frequency band; the real-time primary frequency of pump is accurately extracted by employing the Pauta criterion.
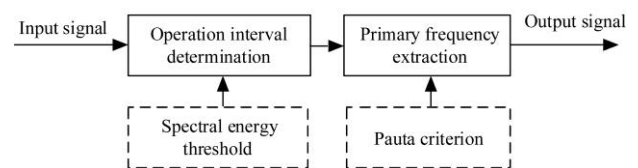

Figure 4　Pump operation status and primary frequency extraction model

3.2.1 Operation interval determination

UAS pump operation status is determined by setting the spectral energy threshold of collected pump signal. Define the collected pump signal as $x(n)$, $n=0$, 1,…, N-1, where n is the

ordinal number and N is the signal length. The result of signal performing the Short-Time Fourier Transform (STFT) is

$$X_n(e^{j\omega}) = \sum_{m=-\infty}^{\infty} x(m) \cdot w(n-m) \cdot e^{-j\omega m} \qquad (4)$$

where, $\{w(n)\}$ is the window sequence; n is the time serial number of frame synchronization; $j^2 = -1$; ω is real variable, $e^{(*)}$ is the exponential operator. Discrete Time domain Fourier Transform (DTFT) of the signal is

$$X(n, e^{j\omega}) = \sum_{m=0}^{N-1} x_n(m) e^{-j\omega m} \qquad (5)$$

Using the discrete Fourier Transform (DFT),

$$X(n,k) = \sum_{m=0}^{N-1} x_n(m) e^{-j\frac{2\pi km}{N}} \qquad (6)$$

where, $k = \omega N / 2\pi$ ($0 \leq k \leq N-1$). $|X(n,k)|$ is the short-time amplitude spectrum of $x(n)$. The spectral energy density function (power spectrum function) $P(n,k)$ at time n is

$$P(n,k) = |X(n,k)|^2 = (X(n,k)) \times (conj(X(n,k))) \qquad (7)$$

where, $conj(*)$ is the conjugate operator. Setting the value of the spectral energy threshold as

$$sum[P(f = 8000:16000)]_{Threshold}$$

If $P(n, k = 8000:16000)$ at time m exceeds the value of $sum[P(f = 8000:16000)]_{Threshold}$, the pump status at time m is recognized. It should be noted that the energy threshold value should be adjusted for different pumps, UAS and sampling frequency, windowing time length; the status pump operation without water is considered as operating fault which is not studied in this paper, the operation status is only divided into two modes (on and off).

3.2.2 Primary frequency extraction

The Pauta Criterion was employed to extract the pump primary frequency during UAS spraying. The rotation speed of diaphragm pump is 20-80 Hz, so is the pump primary frequency. To erase the influence of twice primary frequency (when primary frequency $f \in [20:40)$, see Figure 5 in the following), we first divide the analysis frequency band into two parts, [20:40) and [40:80), then take steps as follows

a. Obtain the mean values of two frequency bands [20:40) and [40:80): $Average_1$, $Average_2$;

b. Obtain the standard deviation of two frequency bands [20:40) and [40:80): δ_1, δ_2;

c. Obtain the Maximum value of two frequency bands [20:40) and [40:80): $Max_1\{f(\omega_1)\}$, $Max_2\{f(\omega_2)\}$, then calculate $\dfrac{|Max_i\{f(\omega_i)\} - Average_i|}{\delta_i} = \beta_i, i = 1,2$, where, β_i is the correlation coefficient of primary frequency determination. In the research of Rough deviation, it is adopted that $\beta_i > \beta_{Threshold} = 3$ (i.e., the 3δ criterion). ω_i is set as the pump primary frequency if $\beta_i > \beta_{Threshold}$. It is noted that the subscripts 1 and 2 refer to frequency bands [20:40) and [40:80) respectively.

4 Pump voice signal analysis

To determine the windowing time length of collected voice signal, and verify the feasibility of the proposed operation status and primary frequency extraction model, finished ground and flight tests are introduced in this section. During the tests, one certain pump used in 8-rotor plant-protection UAS MG-1s was adopted.

4.1 Windowing time length determination

The pump voltage is set 9 V (low-voltage state), the rotation speed of the pump motor is measured 34.63 r/s by Stroboscopic velocimeter (DT2240B, measurement error 1 Hz). Extract pump voice signal of 0.05 s, 0.1 s, 0.2 s, 0.5 s, 1 s, and 2 s length is extracted for Fast Fourier Transform (FFT) analysis, from the microphone placed on pump head. The results are shown in Figure 5 and Table 1.

Figure 5   Effect of windowing time length on primary frequency extraction

As is shown in Figure 5, multiple extreme points (peaks) number of the FFT result changes with different windowing time lengths t. The extreme points number and curve of the FFT results become stable when $t > 0.2$ s. To make detailed comparison between different FFT results, first 4 extreme points of each sub-figure are extracted in Figure 5 and put them in Table 1.

It is seen from Table 1 that the extracted frequency of the 1st extreme point is close to the measured rotation speed (34.63 r/s) when $t > 0.2$ s. It is also seen that the extracted primary of the 1st extreme point with different windowing time length $t = 0.5$ s, 1 s, and 2 s is minimal. When $t = 0.5$ s, 1 s, and 2 s, the value of 2nd extreme point f_2 is twice as much as that of 1st extreme point f_1; similarly, f_3 is triple of f_1, f_4 is fourfold of f_1.

Table 1   Results of frequency extraction

	Windowing time length/s					
	0.05	0.1	0.2	0.5	1	2
f_1	35.62	40.24	34.76	34.91	34.37	35.02
f_2	71.3	70.42	69.51	69.82	68.75	69.05
f_3	107	100.6	104.3	104.7	104.1	104.1
f_4	-	-	139	137.6	138.5	138.1

Note: f_i is the frequency of ith extreme point of FFT results, i=1, 2, 3, 4.

4.2   Pump operation status determination and primary frequency extraction

To verify the feasibility of the operation status and primary frequency determination model, the pump voice collected from 8-rotor plant-protection UAS MG-1s during flight was analyzed. The pump primary frequency was measured before 8-rotor UAS MG-1s took off, which was 61.00 Hz (voltage 14 V, high-voltage state). The windowing time length is set 0.74 s (sampling frequency is 44.1 kHz, Frame length N=32768), the spectral energy threshold $sum[P(f = 8000:16000)]_{Threshold} = 10^4$ dB. Obtained results are shown in Figure 6. It is observed that by setting the spectral energy threshold, the pump operation starting and ending points are determined during the UAS flight.

The pump voice signal during UAS flight is collected and spectrogram analyzed, and the results of 12 s are shown in Figure 7.
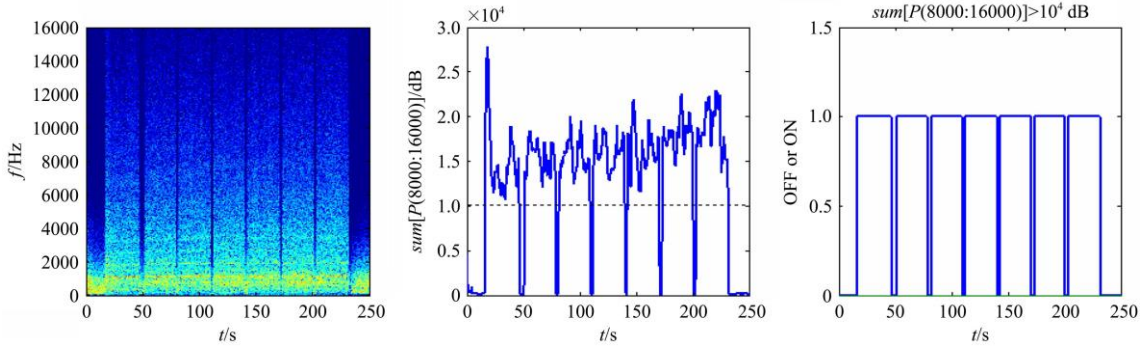

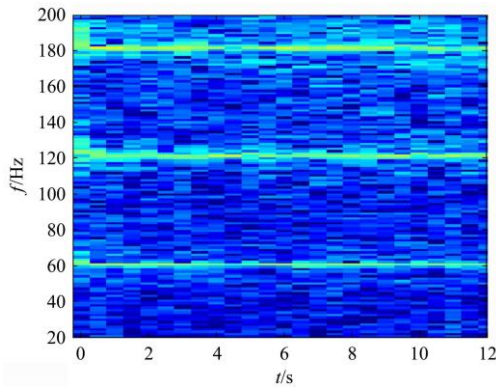Figure 6   Pump operation interval determination during UAS flight

Figure 7   Spectrogram of pump the voice signal of 8-rotor UAS during flight
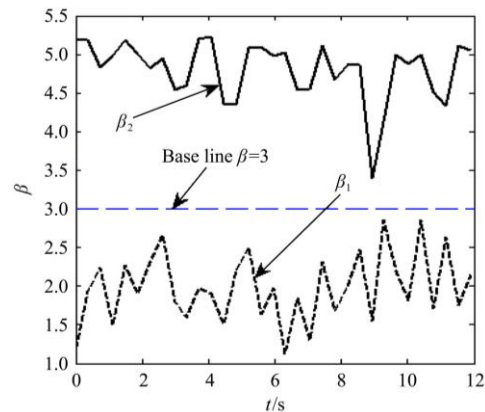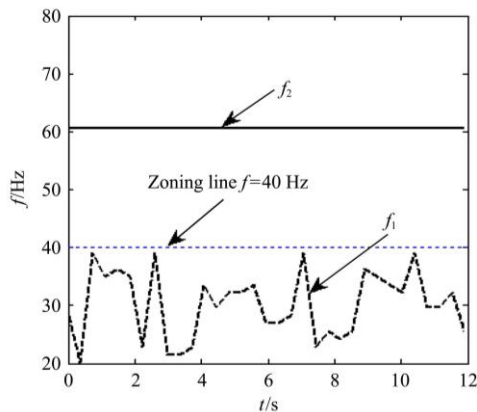
The time-varying regularities of ω_1, ω_2, β_1, β_2 of $Max_1\{f(\omega_1)\}$, $Max_2\{f(\omega_2)\}$ from corresponding frequency bands [20:40) and [40:80) is analyzed , results are shown in Figure 8. It is seen from Figure 8 that the primary frequency is stable and f=61.03 Hz when $\beta_{Threshold}$=3. The max(β_1), min(β_2) of another six sets of pump voice signal from the same flight are calculated, results are shown in Table 2. It is observed from the Table 2 that when we set $\beta_{Threshold}$=3, primary frequency is in the [40:80) frequency band.

Table 2 $Max(\beta_1)$, $Min(\beta_2)$ of pump voice signal

	1	2	3	4	5	6
max(β_1)	2.80	2.72	2.63	2.75	2.66	2.73
min(β_2)	3.20	3.16	3.32	3.27	3.02	3.10

Figure 8   Time-varying regularities of ω_1, ω_2, β_1, β_2 of $Max_1\{f(\omega_1)\}$ and $Max_2\{f(\omega_2)\}$ of 8-rotor UAS

5   Results and discussions

In the following, one certain pump used in 4-rotor plant-protection UAS 3WQFTX-1011S is analyzed. The pump nameplate writes that the rated power is 60 W, maximum pressure is 0.8 MPa and the maximum flow rate is 5 L/min.

5.1 Pump flowrate fitting surface

To acquire the pump flowrate formulas at different rotation speed (i.e., primary frequency) under different nozzle combinations, 4 kinds of nozzle combinations are employed during the test: F110-02*2, F110-01*2+F110-015*2, F110-015*4, F110-015*2+ F110-02*2 (measured outlet areas are 1.23 mm^2, 1.52 mm^2, 1.89 mm^2 and 2.10 mm^2, respectively). During the flowrate data collecting process, stroboscopic velocimeter (DT2240B) was used to determine the rotation speed of the pump motor; electronic balance (YHC-L01, maximum weighing 30 kg) was used to measure the spray amount under different rotation speeds and outlet areas (i.e., different nozzle combinations). The vertical distance between the nozzles and pump is strictly less than 0.5 m. Pump pressure knob is twisted to the end during the collection tests and in the following.   The obtained flowrate surface is shown in Figure 9.

The fitting formulas is

$$S_{re}(n, A) = -7.052 - 2.745A + 0.7197f + 2.389A^2$$
$$-0.01202A \cdot f - 0.01743f^2 - 0.5648A^3 \qquad (8)$$
$$+ 0.001213A^2 \cdot f + 0.0003414A \cdot f^2 + 0.0001371f^3$$

The SSE (sum of squares due to error) of the fitting formula is 0.008149, which is close to zero.   It is seen from Figure 9 that pump flowrate increases as rotation speed and outlet area increase. To verify the fitting accuracy, comparative tests are carried out using another two nozzle combinations: F110-015*3, F110-015*3+ F110-02*1 (the measured outlet areas are 1.38 mm^2, 1.92 mm^2), obtained results are shown in Table 3.
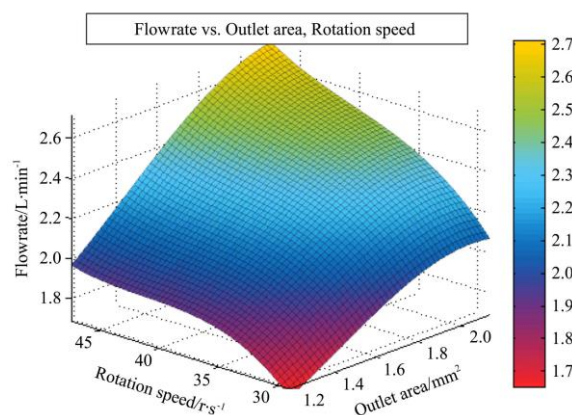

Figure 9   Fitting surface of spray flowrate with pump rotation speed and outlet area

Table 3   Comparison of measured and fitted results of spray flowrate

Measured outlet area A/mm^2		Rotation speed of pump motor/r s^{-1}						Maximum deviation rate
		30.00	33.33	36.67	40.00	43.33	46.67	
1.38	Measured flowrate/L min^{-1}	1.79	1.98	2.04	2.06	2.11	2.17	2.8%
	Fitted flowrate/L min^{-1}	1.80	1.95	2.03	2.06	2.08	2.11	
1.92	Measured flowrate/L min^{-1}	2.14	2.30	2.40	2.49	2.56	2.61	1.7%
	Fitted flowrate/L min^{-1}	2.12	2.29	2.39	2.46	2.51	2.59	

It is observed from Table 3 that similar to result in Figure 9, spray flowrate increases as outlet area or rotation speed increases. When A=1.92 mm^2, the fitted flowrate is not stable: the fitted flowrate value exceeds the measured one when rotation speed< 40 r/s, while fitted flowrate value is less than measured one when rotation speed>40 r/s.   However, when A=1.38 mm^2, fitted flowrate value remains less than measured one.   But the maximum deviation rate of fitted spray flowrate is only 2.8%, which attains high fitting degree.

5.2   Flight tests of UAS spraying under manual and autonomous control

To determine the measurement accuracy of flowrate monitoring system, the following tests were conducted in Henan Anyang test base.   4-rotor Plant-protection UAS 3WQFTX-1011S was used under manual control and autonomous control. Two nozzle combinations were employed during the test: F110-010*4 and F110-015*4. The flowrate of different nozzle combinations was measured by electronic balance (YHC-L01) before flight.   To measure the total spray amount, we recorded the weight of the UAS before take-off and after landing, measured by portable electronic scale (WeiHeng, maximum weighing 50 kg).   Stopwatch was used to record each time when the pilot turned on/off the UAS pump operating switch.   During the tests, we set sampling frequency as 44.1 kHz, frame length N = 32768, spectral energy threshold $sum[P(f$=8000:16000]$_{Threshold}$=3×10^4 dB, $\beta_{Threshold}$=3.

5.2.1   Flight tests of UAS spraying under manual control

In this test, 4-rotor plant protection UAS 3WQFTX-1011S was used in manual flight control mode.   Four nozzles of F110-010 at UAS first flight were installed, and four F110-015 nozzles at another two flights.   Employing the pump operation status determination model, endpoints extracted from the collected signals are shown in Figure 10.

It is seen from Figure 10 that, the spectral energy of collected signal remain less than the threshold during take-off, flight without spraying and landing, so the spraying status remains zero at those intervals; when the pump operates during the flight, the spectral energy exceeds the threshold and the spraying status changes to 1. The spectral energy expands quickly and greatly, at the very beginning of pump operating of each time.   However, at third flight, the spectral energy comes close to the threshold value in the latter part of UAS flight spraying.   It means the extracted endpoints are sensitive to the spectral energy threshold, which shouldn't be set too high or low.   The extracted flowrate is stable during UAS flight, which remains invariable at the same flight. And the flowrate also remains invariable at different flights under the same outlet area (i.e., the second and third flight).   Recognized endpoints by setting spectral energy threshold and recorded pump switch time by stopwatch are shown in Table 4.

It is clearly observed from Table 4 that, the deviation of endpoints between extracted results and recorded results is low. Each extracted starting/end point is head of the recorded, the max deviation of starting point is 0.7 s, the max deviation of end point is 0.7 s.   While the extracted total time is close to the recorded results, the max deviation is only 0.8 s.   Which performs better than that using double-threshold model (max deviation 2 s)[27]. The extracted Spray flowrate and total spray amount by Pump operation status and primary frequency extraction model are shown in Table 5.

As seen from Table 5, the extracted spray flowrate is close to the recorded value, and the deviation of extracted spray flowrate

is less than 2%. However, the total spray amount tends to deviate away from the recorded value, i.e., deviation rate of total spray amount is higher than that of spray flowrate. It is because of the endpoints recognition deviation mentioned in Table 4. Different from the result of spray flowrate, the extracted total spray amount values all exceed those of recorded values. While the max deviation rate of total spray amount is still low (3.2%).
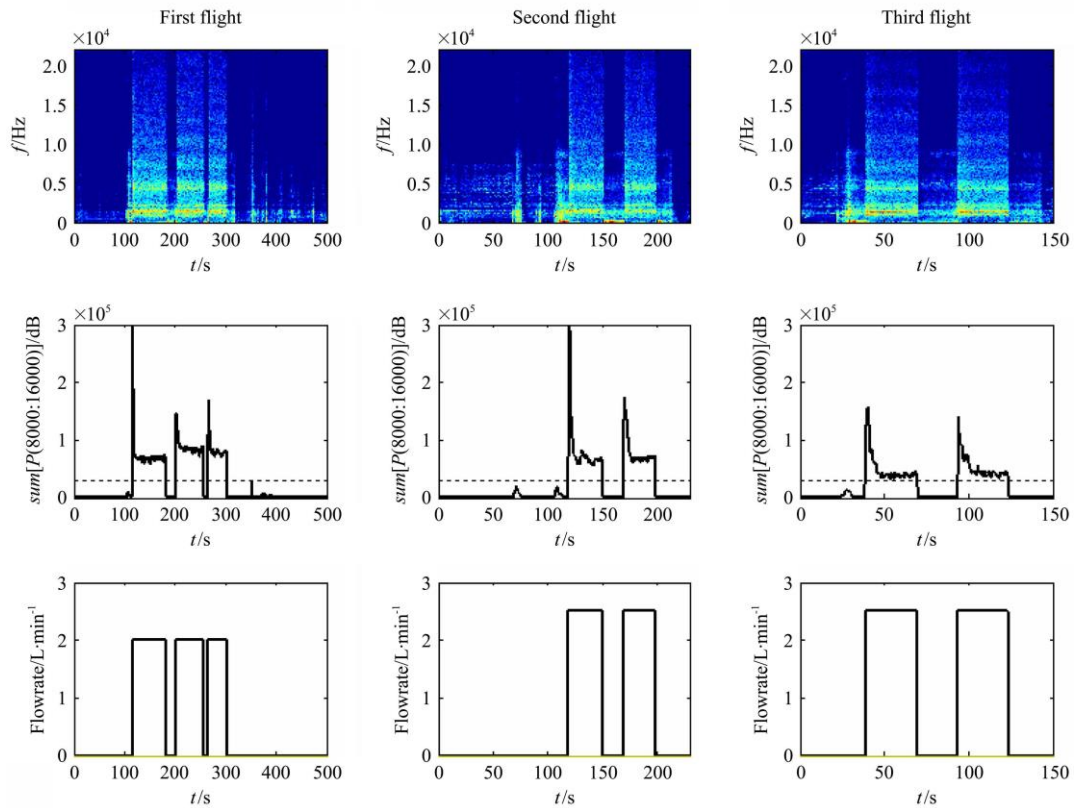

Figure 10   Recognized pump flowrate during UAS flight by setting spectral energy threshold under manual control

Table 4   Endpoints recognized by setting spectral energy threshold and recorded by stopwatch

Flights	Extracted results by setting spectral energy threshold			Results recorded by stopwatch			Deviation	
	Starting/s	End/s	Operation time/s	Starting/s	End/s	Operation time/s	Starting deviation/s	End deviation/s
1	115.7	182.8	67.1	115.9	183.5	67.6	0.2	0.7
	202.8	256.3	53.5	202.8	256.7	53.9	0	0.4
	266.4	303.2	36.8	267.1	303.6	36.5	0.7	0.4
	Total recognized time/s		157.4	Total recorded time/s		158.0	Total Deviation/s	0.6
2	119.3	150.4	31.1	119.4	151.0	31.6	0.1	0.6
	169.8	198.9	29.1	170.0	199.4	29.4	0.2	0.5
	Total recognized time/s		60.2	Total recorded time/s		61.0	Total Deviation/s	0.8
3	38.7	70.2	31.5	39.0	70.6	31.6	0.3	0.4
	94.5	123.4	28.9	94.7	124.0	29.3	0.2	0.6
	Total recognized time/s		60.4	Total recorded time/s		60.9	Total Deviation/s	0.5

Note: The reaction time was ignored during recording the time of pilot turning on/off the pump switch by stopwatch.

Table 5   Spray flowrate and total spray amount recognized by extraction model and recorded by graduated cylinder, portable electronic scale

Flights	Spray flowrate			Total spray amount		
	Extracted value/L min^{-1}	Recorded value/L min^{-1}	Deviation rate/%	Extracted value/L	Recorded value/L	Deviation rate/%
1	2.00	1.99	0.5	5.29	5.20	1.7
2	2.50	2.53	1.2	2.56	2.48	3.2
3				2.55	2.50	2.0

5.2.2   Flight tests of UAS spraying under autonomous control

Autonomous flight control mode of 4-rotor plant protection UAS 3WQFTX-1011S was adopted in this test. Four F110-010 nozzles are installed at the first flight, and four F110-015 nozzles at the second flight. The spray is automatically on if UAS' horizontal speed exceeds 3 m/s. In this test, portable electronic scale (Weiheng) was used to measure the total spray amount. Extracted endpoints and Flowrate results are shown in Figure 11 and Table 6.

Table 6   Total spray amount recognized by extraction model and recorded by portable electronic scale

Flights	Extracted value/L·min⁻¹	Recorded value/L·min⁻¹	Deviation rate
1	1.61	1.64	1.8%
2	5.28	5.30	0.4%

In Figure 11, each spraying interval and flowrate of first flight or the second can be tracked.   And the extracted flowrate remains constant in the same flight, under the same outlet area.   It is seen from Table 6 that the difference between the extracted total spray amount and the recorded is low, the deviation rate is less than 2%.
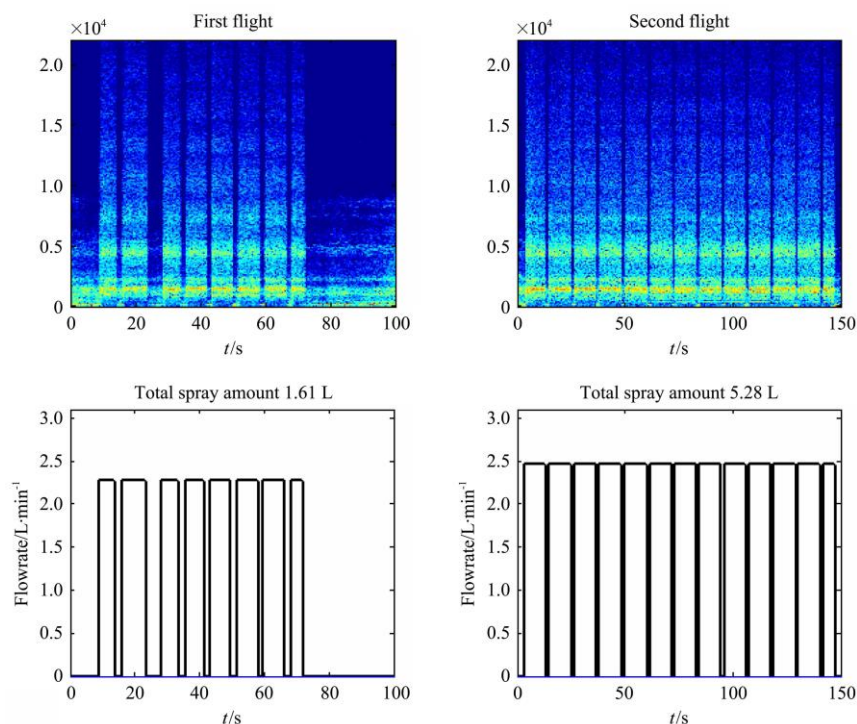

Figure 11   Extracted endpoints during UAS flight under autonomous control

6   Conclusions

A STM32-based monitoring system was designed to acquire the pump operating status and operating primary frequency during UAS flight based on the collected pump voice.   In pump voice analysis test, the extracted primary frequency (i.e., the rotation speed of pump motor) comes close to the measured value by Stroboscopic velocimeter when microphone placed on the pump head and voice windowing time length $t>0.2$ s; the error rate of the extracted pump primary frequency is less than 1% when windowing time length $t=0.74$ s.   A pump operation status and primary frequency extraction model was proposed based on collected pump voice analysis.   In the test, 8-rotor plant-protection UAS MG-1s operating status was determined, by setting the spectral energy threshold $sum[P(f=8000:16000]_{Threshold}=10^4$ dB; employing the Pauta criterion, the extracted UAS pump primary frequency of UAS pump was close to measured value during UAS flight spraying (difference is only 0.03 Hz).   The operating status of 4-rotor UAS 3WQFTX-1011S is determined by setting energy threshold $sum[P(f=8000:16000]_{Threshold}=3\times10^4$ dB, the max deviation of operating starting/end point is only 0.7 s and the max deviation of extracted total operating time is only 0.8 s.

A flowrate fitting formula of 4-rotor plant protection UAS 3WQFTX-1011S was obtained under different outlet area and pump primary frequency.   In the comparative test, the max deviation rate of fitted spray flowrate is only 2.8%.   In the UAS flight tests under manual and autonomous control, the monitoring system could output the real-time values of spray flowrate and amount, each operating interval and flowrate during flight could be visually tracked; the deviation of extracted spray flowrate is less than 2%, and the maximum deviation rate of total spray amount is 3.2%.

[References]

[1]   He X K, Bonds J, Herbst A, Langenakens J.   Recent development of unmanned aerial vehicle for plant protection in East Asia.   Int J Agric & Biol Eng, 2017; 10(3): 18–30.

[2]   Yang S L, Yang X B, Mo J Y.   The application of unmanned aircraft systems to plant protection in China.   Precision Agriculture, 2018; 19: 278–292.

[3]   Xue X Y, Lan Y B, Sun Z, Chang C, Hoffmann W C.   Develop an unmanned aerial vehicle based automatic aerial spraying system. Computers and Electronics in Agriculture, 2016; 128: 58–66.

[4]   Qin W C, Qiu B J, Xue X Y, Chen C, Xu Z F, Zhou Q Q.   Droplet deposition and control effect of insecticides sprayed with an unmanned aerial vehicle against plant hoppers.   Crop Protection, 2015; 85: 79–88.

[5]   Yallappa D, Veerangouda M, Maski D, Palled V, Bheemanna M. Development and evaluation of drone mounted sprayer for pesticide applications to crops.   2017 IEEE Global Humanitarian Technology Conference (GHTC), 2017; pp.19–22.

[6]   Iwasaki K, Torita H, Abe T, Uraike, T, Touze M, Fukuchi M, et al. Spatial pattern of windbreak effects on maize growth evaluated by an unmanned aerial vehicle in Hokkaido, northern Japan.   Agroforest Syst, 2018.   doi: 10.1007/s10457-018-0217-7.

[7]   Xue X Y, Tu K, Qin W C, Lan Y B, Zhang H.   Drift and deposition of ultra-low altitude and low volume application in paddy field. International Journal of Agriculture and Biology, 2014; 7(4): 23–28.

[8]   Zheng Y, Yang S, Zhao C, Chen L, Lan Y, Tan Y.   Modelling operation parameters of UAV on spray effects at different growth stages of corns. Int J Agric & Biol Eng, 2017; 10(3): 57–66.

[9]   Wen S, Zhang Q, Deng J, Lan Y B, Shan J.   Design and experiment of a variable spray system for unmanned aerial vehicles based on PID and PWM control.   Applied Sciences, 2018; 8(12): 2482.   doi: 10.3390/app8122482.

[10]   Lian Q, Tan F, Fu X, Liu X, Zhang P, Zhang W.   Design of precision variable-rate spray system for unmanned aerial vehicle using automatic control method.   Int J Agric & Biol Eng, 2019; 12(2): 29–35.

[11]   Wang S L, Song J L, He X K, Song L, Wang X N, Wang C L, et al. Performances evaluation of four typical unmanned aerial vehicles used for pesticide application in China.   Int J Agric & Biol Eng, 2017; 10(4): 22–31.

[12]   Wang C L, He X K, Wang X N, Wang Z C, Wang S L, Li L L, et al. Testing method and distribution characteristics of spatial pesticide spraying deposition quality balance for unmanned aerial vehicle.   Int J Agric & Biol Eng, 2018; 11(2): 18–26.

[13]   Yang F B, Xue X Y, Cai C, Sun Z, Zhou Q Q.   Numerical simulation and analysis on spray drift movement of multirotor plant protection unmanned aerial vehicle.   Energies, 2018; 11(9): 2399.   doi: 10.3390/en11092399

[14]   Zhang B, Tang Q, Chen L P, Xu M.   Numerical simulation of wake vortices of crop spraying aircraft close to the ground.   Biosystems Engineering, 2016; 145: 52-64.

[15]   Wang L, Chen D, Zhang M, Wu Y, Yao Z, Wang S.   CFD simulation of low-attitude droplets deposition characteristics for UAV based on multi-feature fusion.   IFAC-PapersOnLine, 2018; 51(17): 648–653.

[16]   Hunt E R, Hively W D, Fujikawa S J, Linden D S, Daughtry C S T, McCarty G W.   Acquisition of NIR-green-blue digital photographs from unmanned aircraft for crop monitoring.   Remote Sensing, 2010; 2: 290–305.

[17]   Salam í E, Barrado C, Pastor E.   UAV flight experiments applied to the remote sensing of vegetated areas.   Remote Sensing, 2014; 6:

11051–11081.

[18]   Collacott R A.   The identification of the source of machine noises contained within a multiple－source environment.   Applied Acoustics, 1976; 9(3): 225–238.

[19]   Ota Y, Wilamoski B M.   Identifying cutting sound characteristics in machine tool industry with a neural network.   IEEE International Conference on Neural Networks-Conference Proceedings, 1998; 3(3): 2459–2464.

[20]   Lin J.   Feature extraction of machine sound using wavelet and its application in fault diagnosis.   NDT & E International, 2001; 34(1): 25–30.

[21]   Li Z, Ren L, Shi Y.   A humanoid method for extracting abnormal engine sounds from engine acoustics based on adaptive Volterra filter.   Journal of Bionic Engineering, 2012; 9(2): 262–270.

[22]   Mannan M A, Kassim A A, Jing M.   Application of image and sound analysis technique to monitor the condition of cutting tool.   Pattern Recognition Letters, 2000; 21(11): 969–979.

[23]   Anami B S, Pagi V B.   Acoustic signal based detection and localisation of faults in motorcycles.   IET Intelligent Transport Systems, 2014; 8(4): 345–351.

[24]   He X K.   Rapid development of unmanned aerial vehicles (UAV) for plant protection and application technology in China.   Outlooks on Pest Management, 2018; 29(4): 162–167.

[25]   Ru Y, Zhou H P, Fan Q N, Wu X W.   Design and investigation of ultra-low volume centrifugal spraying system on aerial plant protection. ASABE International Meeting, Louisville, Kentucky, 2011.   doi: 10.13031/2013.37266.

[26]   Yang K, Yang G Y, Fu H.   Research of control system for plant protection UAV based on Pixhawk.   Procedia Computer Science, 2020; 166: 371–375.

[27]   Xu Y, Xue X Y, Sun Z, Gu W, Chen C, Jin Y K, et al.   Online spraying quality assessment system of plant protection unmanned aerial vehicle based on Android client.   Computers and Electronics in Agriculture, 2019; 166: 104938.   doi: 10.1016/j.compag.2019.104938